Available online at www.sciencedirect.com
SCIENCE DIRECT®
International Journal of Heat and Mass Transfer 47 (2004) 3825–3840
International Journal of HEAT and MASS TRANSFER
www.elsevier.com/locate/ijhmt

Direct-contact evaporation in the homogeneous and heterogeneous bubbling regimes. Part I: experimental analysis

Cláudio P. Ribeiro Jr., Paulo L.C. Lage *

Programa de Engenharia Química—COPPE, Universidade Federal do Rio de Janeiro P.O. Box 68502, 21945-970 Rio de Janeiro, RJ, Brazil

Received 5 June 2003; received in revised form 15 March 2004
Available online 6 May 2004

Abstract

Using the air–water system, transient experimental measurements of liquid temperature, bubbling height, evaporation rate, gas hold-up and bubble size distributions in a direct-contact evaporator were performed for four gas superficial velocities including operation in both homogeneous and heterogeneous bubbling regimes. Perforated and porous plates were used as spargers. Significant effects of both the sparger and the gas flow rate upon the equipment performance were verified and systematically analysed, revealing some rather interesting features of transient non-isothermal bubbling, such as temporal evolution of bubble size distributions and gas hold-up values.

Keywords: Heat and mass transfer; Direct-contact evaporation; Gas hold-up; Bubble; Bubble column

1. Introduction

Direct-contact evaporators constitute an example of the different kinds of equipment which comprise the class of the so-called direct-contact heat exchangers, whose main feature is the lack of any walls separating the processing streams [1,2]. The heating fluid, a superheated gas, is dispersed as bubbles in the solution to be concentrated. Owing to this absence of intervening walls, direct-contact evaporators exhibit many advantages over the traditional shell-and-tube units, among which one can highlight higher thermal efficiency, decreased capital investment, lower operating and maintenance costs, greater simplicity of construction and the possibility to operate economically with highly fouling and/or corrosive solutions. Industrially, this kind of evaporator has already been used, for instance, for concentrating aqueous solutions of phosphoric acid, sulphuric acid, sodium hydroxide and calcium chloride, to name but a few [3,4].

The equipment is basically constituted of a liquid column through which a superheated gas is bubbled. In other words, it can be described as a non-isothermal bubble column. The sparger, responsible for bubble formation, is located at the bottom of the column. Perforated plates or a set of perforated pipes are commonly employed as spargers. When the gaseous stream is composed of combustion products, usually generated in a combustion chamber located inside the liquid phase, the unit is more frequently known as a submerged combustion evaporator.

Since the gas is superheated, there exists a natural energy flux from the interior to the surface of the bubbles during both the formation and the ascension stages, which generally accounts for most but not all the energy received by the liquid. The remaining energy amount is transferred through the gas chamber walls, including the sparger. This energy can be transferred either as sensible heat, leading to a temperature rise, or as latent heat,

* Corresponding author. Tel.: +55-21-2562-8346; fax: +55-21-2562-8300.
E-mail address: paulo@peq.coppe.ufrj.br (P.L.C. Lage).

0017-9310/$ - see front matter © 2004 Elsevier Ltd. All rights reserved.
doi:10.1016/j.ijheatmasstransfer.2004.03.018

Nomenclature

A_c	Evaporator cross section area (m^2)
A_i	interfacial area (m^2)
Cp	specific heat at constant pressure ($J\,kg^{-1}\,K^{-1}$)
d_{30}	volumetric mean bubble diameter (m)
d_{32}	Sauter mean bubble diameter (m)
d_{cor}	volumetric mean bubble diameter predicted by literature correlations (m)
d_e	equivalent diameter of the sphere with the same volume of the bubble (m)
D_c	evaporator inner diameter (m)
H_b	two-phase mixture overall height in the evaporator (m)
H_o	pure liquid height in the column (m)
ΔH_{vap}	latent heat of vaporisation ($J\,kg^{-1}$)
m_L	liquid mass in the evaporator (kg)
M	mass flow rate ($kg\,s^{-1}$)
Q	heat transfer rate (W)
P	pressure (Pa)
RF	relative frequency
t	time (s)
T	temperature (K)
ΔT_{bl}	boiling point raise (K)
u_G	gas superficial velocity ($m\,s^{-1}$)
U	overall heat-transfer coefficient ($W\,m^{-2}\,K^{-1}$)

Greek symbols

α	area for inter-phase transfer processes per cross section area of the column
ε	gas hold-up
ρ	density ($kg\,m^{-3}$)

Subscripts

bf	predicted from bubble formation models
d	sparger
ev	evaporated from the liquid phase
G	gas
I	injected gas
L	liquid
p	losses from the liquid phase to the surroundings
T	total

Superscripts

in	stream entering the evaporator
out	stream leaving the evaporator

bringing about vaporisation and thereby originating a mass flux from the surface to the interior of the bubbles. The amount of a liquid component which can be transferred to the dispersed phase is proportional to its vapour pressure [5] and, hence, the higher the temperature of the liquid, the greater the fraction of the total energy transferred as latent heat. Eventually, an equilibrium temperature is reached, at which almost all the energy is used in the vaporisation, being the sensible heat fraction only responsible for compensating the heat losses of the unit.

The concept of direct-contact evaporation itself is by no means new, as the early attempts at designing apparatus based on it date back to the 19th century [6]. Nonetheless, there has been little published work which can be directly employed in the design of direct-contact evaporators. From the literature, most of the experimental studies concerning the subject were aimed at illustrating the viability of applying the technique to concentrate different solutions whose treatment in conventional evaporators would be cumbersome, and emphasis was given only to the quasi-steady-state evaporation rate for different operating conditions [5–10]. The effect of some operating variables on the performance of an experimental unit has already been reported by Iyer and Chu [11] and Kawasaki and Hayakawa [12]. However, the only available data set for the dynamic operation of a direct-contact evaporator seems to be the one presented by Queiroz [13], who worked with combustion products as the dispersed phase and employed both water and an aqueous sodium chloride solution as the continuous phase for a pilot unit 0.57 m in diameter. The unit operation was limited to the homogeneous bubbling regime, in which there is little variation in the size of the bubbles and the breakage and coalescence phenomena are negligible [14–16]. Industrially, however, the homogeneous regime is less likely to prevail, owing to the high gas flow rates employed, which favour the heterogeneous bubbling regime, characterised by a wide range of bubble sizes and considerable frequencies of breakage and coalescence. It should be emphasised that data sets for the dynamic operation of direct-contact evaporators are of fundamental importance for validating any kind of mathematical model for this equipment that takes the transient behaviour of the continuous phase into account, which, in turn, constitutes a useful tool for design.

Based upon the aforementioned aspects, the necessity of additional experimental data on direct-contact evaporation is evident, particularly insofar as the heterogeneous bubbling regime is concerned. Therefore, in this work, aiming at providing a better characterisation of the heat and mass transfer processes which take place in a direct-contact evaporator, experimental runs were

conducted in a bench scale unit with the air–water system. Transient values of liquid temperature, evaporation rate, bubbling height and gas hold-up were measured in duplicate for each considered operating condition. Two different spargers and four gas superficial velocities were considered, enabling the operation in both homogeneous and heterogeneous regimes.

2. Materials and methods

2.1. Experimental set-up

The set-up used for conducting the experiments is shown in Fig. 1. The system was fed with dry compressed air (dew point at 273 K) and three parallel rotameters were available for flow rate measurements, whose error is estimated to be about 5%. In all runs, the gauge pressure in the air line was kept at 4 bar.

The air stream was heated in an electrical oven with a total power of 2000 W, in which the air flowed in a AISI 316 stainless steel serpentine with a nominal diameter of 1/4 in and a length of 23 m, at the centre of which the cylindrical, ceramic heating element of the oven was located. The heating element had ten shallow gutters evenly distributed along its transversal section, in which the electrical resistances were placed, being in direct contact with the air in the oven. The serpentine/heating element set was insulated with refractory bricks and ceramic fibre (Kaowool® 1260). A thermocouple type K registered the oven operating temperature, whose value was always kept below the working limit of AISI 316 stainless steel (925 K) by means of an on-off control system of the voltage applied to the electrical resistances.

The pipeline which connected the oven and the evaporator was thoroughly insulated with ceramic fibre. Aiming at minimising heat losses, an electrical resistance with an overall power equal to 160 W was coiled around this part of the pipeline. The gas temperature was measured both at the oven outlet and in the chamber beneath the sparger using thermocouples type K, whose sensors were located in the middle of the pipes cross section with the aid of tee fittings. After the first thermocouple there was a needle valve for controlling the air flow rate in the by-pass line used during the transient heating of the oven. Beyond this valve there existed another needle valve which controlled the gas flow rate fed to the equipment.

The evaporator itself consisted of a glass column 7.3 cm in inner diameter and 0.7 m in height, at the bottom of which the sparger was placed, and whose top was closed with an aluminium lid sealed with Viton® O-rings. A platinum resistance thermometer (PT-100), 1.0 m in length, was placed in this lid for measuring the temperature of the liquid. The gas stream from the evaporator was sent to two glass Graham condensers for

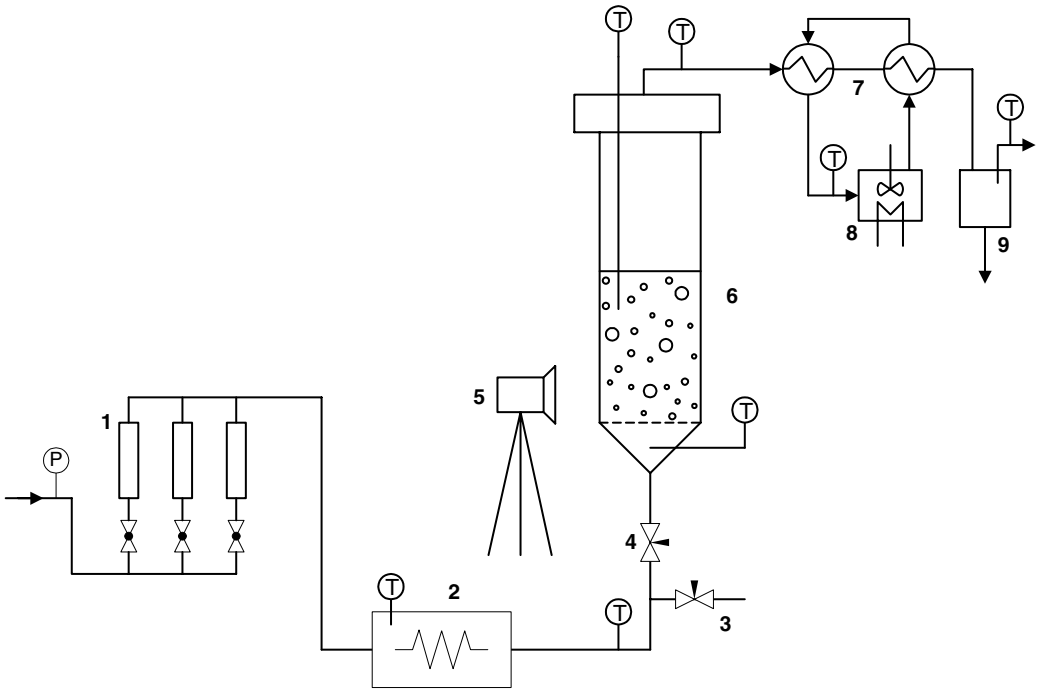

Fig. 1. Schematic diagram of the experimental setup: (1) rotameters, (2) electrical oven, (3) by-pass valve, (4) main valve, (5) photographic camera, (6) evaporator, (7) condensers, (8) circulating bath, (9) flask for collecting condensate.

condensing the evaporated water, which was collected in a two-neck flask (provided with a stopcock outlet) and subsequently weighed in an analytical standard balance (Ohal®, model AS120). The condensers were fed with water at 278 K as cold fluid, provided by a refrigerating circulator.

The gas distribution system was composed of two sintered AISI 316 stainless steel plates 3.24 and 2.19 mm in thickness, both with a diameter of 8.0 cm. Different regions of the surface of the thinner plate, which was in contact with the liquid during operation, were analysed in a scanning electron microscope (JEOL®, model JSM-5300) and a mean pore diameter of (12 ± 5) μm was determined for this plate. On top of this porous plate, an AISI 316 stainless steel perforated plate could be used, 0.53 mm in thickness and 8.0 cm in diameter, containing 89 orifices with a diameter equal to 0.5 mm arranged in a quadrangular pattern with a pitch of 6.3 mm. The desired set of plates was fixed between two flanged aluminium pieces, being the glass column fitted into the upper aluminium piece, in which there was an outlet pipe for liquid removal. The system was sealed with Viton O-rings and graphoil. The bottom of the column was rested on insulating bricks, which were covered with ceramic fibre to increase the efficiency of the thermal insulation.

The lateral area of the evaporator was insulated with a glass fibre piece for pipe insulation which had been divided into two equal parts. One half was fixed to the column wall and a graduated scale was glued on it for measuring the overall height of the mixture in the column. The other half, attached to the first one, could be moved by rotation for photographing the two-phase mixture and reading its overall height. All photographs were taken with a SONY digital camera (model MAVICA® MVC-FD91), adjusting the setting of the shutter speed to 10^{-3} s so that the required illumination was provided by the camera flash.

2.2. Experimental procedure and data processing

All experiments were performed with the air-distilled water system. At the beginning of each run, the evaporator feeding valve was closed and the by-pass valve was opened to the desired air flow rate. The electrical oven was turned on and while it reached its steady-state temperature, the photographic camera was appropriately positioned. When the gas operating temperature had been achieved, a previously weighed mass of liquid was poured into the column, the liquid height without bubbling was recorded and, then, the heating resistance of the pipe between the oven and the evaporator was turned on. The by-pass valve was closed and the evaporator valve was immediately opened to the desired air flow rate, so that bubbling commenced. The overall mixture height was read and the glass fibre insulation was closed.

Periodical readings of the air temperature at the oven outlet and at the column inlet, the liquid temperature, the overall mixture height, the gas outlet temperature and the mass of condensed water were made. Apart from that, aiming at the determination of the bubble size distribution, five pictures of the two-phase mixture in the region close to the sparger (about 0.11 m above it) were taken. The test was conducted until the quasi-steady-state was reached, at which the liquid temperature and the evaporation rate remained approximately constant. Since the initial mass of liquid in the column was known, the values of the liquid temperature and the mass of condensate enabled the calculation of the pure liquid height in the column (H_o) as a function of time by $H_o(t) = 4m_L(t)/\pi D_c^2 \rho_L(t)$, which, in turn, allow the estimation of the gas hold-up in the evaporator using the experimental value of the overall mixture height, H_b, by $\varepsilon = (H_b - H_o)/H_b$.

Aiming at estimating the heat losses from the liquid phase to the surroundings (Q_p), the variation of the liquid temperature after the interruption of the gas feed was monitored. As the liquid mass in the column was known, the heat-transfer rate related to the observed temperature drop could be calculated for each time interval. The mean of the observed values corresponded to Q_p, from which the overall heat-transfer coefficient U_p was determined, adopting, as references, the lateral area of the column containing liquid and the temperature difference between this liquid and the surroundings.

The amount of energy transferred from the sparger to the liquid can be calculated by means of a heat balance of the experimental data for operation in the quasi-steady-state regime. In this regime, since no sensible heat is transferred to the liquid phase, the sum of the heat losses and the latent heat associated with the evaporation rate must equal the amount of energy received by the liquid from the gas and from the sparger. As the level of gas superheating was low, the amount of energy transferred to the liquid can be estimated as $Q_G = M_G Cp_G(T_I - T_L)$, so that the value of Q_d was given by $Q_d = M_{ev}\Delta H_{vap}(T_L) + Q_p - M_G Cp_G(T_I - T_L)$. The individual application of this equation to the experimental data for operation in the quasi-steady-state regime enabled a mean value of Q_d to be determined.

The image analysis for determining bubble sizes and, consequently, bubble size distributions was performed using the software *Tnimage*, version 3.2.0 [17], following the experimental procedure detailed by Ribeiro and Lage [18]. A minimum of 450 bubbles was analysed for each experimental condition in order to guarantee the statistical significance of the determined size distributions, which can be used to calculate several mean bubble diameters, such as the volume to surface mean bubble diameter or Sauter diameter, d_{32}.

Also of interest is the interfacial area, A_i, which depends upon the bubble size distribution, the gas hold-up

and the bubbling height according to $A_i = 6\varepsilon A_c H_b/d_{32}$. A dimensionless interfacial area, α, may be defined by $\alpha \equiv A_i/A_c = 6\varepsilon H_b/d_{32}$, which represents the available area for inter-phase transfer processes per cross section area of the column.

3. Results and discussion

3.1. Effects of the gas flow rate and gas sparger

Initially, using the stainless steel perforated plate as sparger and keeping the initial mass of liquid in the column at a constant value, namely, (1.303 ± 0.005) kg, the effect of the gas flow rate on the operating performance of the evaporator was studied. Experiments in duplicate and in a random order were carried out for four different gas superficial velocities, which were calculated considering the gas to be at the liquid equilibrium temperature (340 K).

The experimental data for the evaporation rate, the liquid-phase temperature and the inlet gas-phase temperature are respectively presented in Fig. 2a–c. In these figures, the filled and open symbols with the same geometrical shape refer to duplicates for the same experimental condition. Regardless of the gas flow rate, the agreement between the duplicates demonstrates an excellent reproducibility of the data.

As shown in Fig. 2a, an increase in the value of u_G leads to an augmentation of M_{ev} in the quasi-steady-state regime, which is consonant with the results of Iyer and Chu [11] and Kawasaki and Hayakawa [12]. This effect steams directly from the larger amount of available energy carried by the gas per unit time as u_G grows, which is also responsible for the decrease in the period of transient operation of the evaporator. Comparing the data shown in Fig. 2b and c, it can be seen that T_G^{in} changes faster than T_L, but not fast enough to allow assumption of constant T_G^{in} during the experimental runs. The apparatus thermal inertia is responsible for the T_G^{in} transient behaviours shown in Fig. 2c.

The data in Fig. 2b also indicate that the quasi-equilibrium value of T_L increases with u_G, an effect which becomes more evident for higher values of u_G. This result could be related to an increase in the operating pressure of the evaporator owing to the pressure drop in the condensers. Since the pressure drop grows with the square of the flowing velocity [19], the higher the gas flow rate, the higher this effect, a fact that is consistent with the tendency observed in Fig. 2b. This hypothesis was verified by performing experimental measurements of the pressure in the column without liquid during air flow at room temperature by connecting a U-type manometer to the outlet pipe in the base of the column. The hydrostatic pressure associated with the mean liquid height in the evaporation experiments (22–27 mbar,

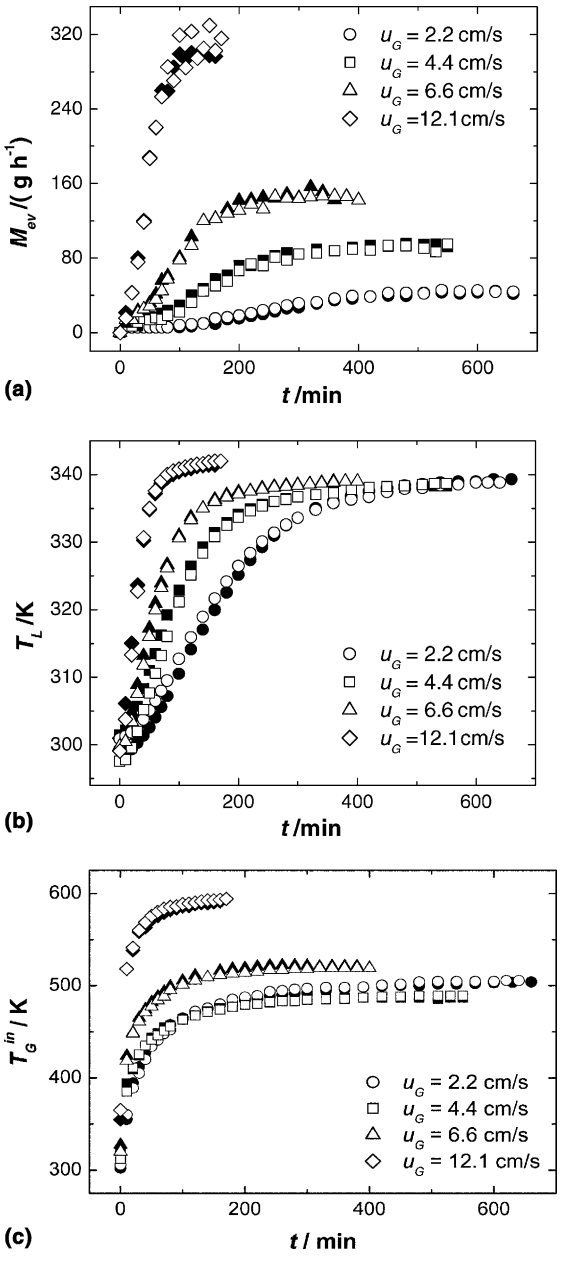

Fig. 2. Transient operation of the direct-contact evaporator for different gas superficial velocities (open and filled symbols refer to duplicates): (a) evaporation rate, (b) liquid temperature and (c) inlet gas temperature.

depending upon u_G) was added to the measured pressure values and the obtained results are shown in Fig. 3a. Confirming the initial hypothesis, the gas flow along the Graham condensers causes the operating pressure in the evaporator to increase significantly with u_G, which is reflected in the quasi-equilibrium value of T_L. In order to illustrate the effect of this pressure variation in terms of T_L, the elevation of the boiling temperature for the

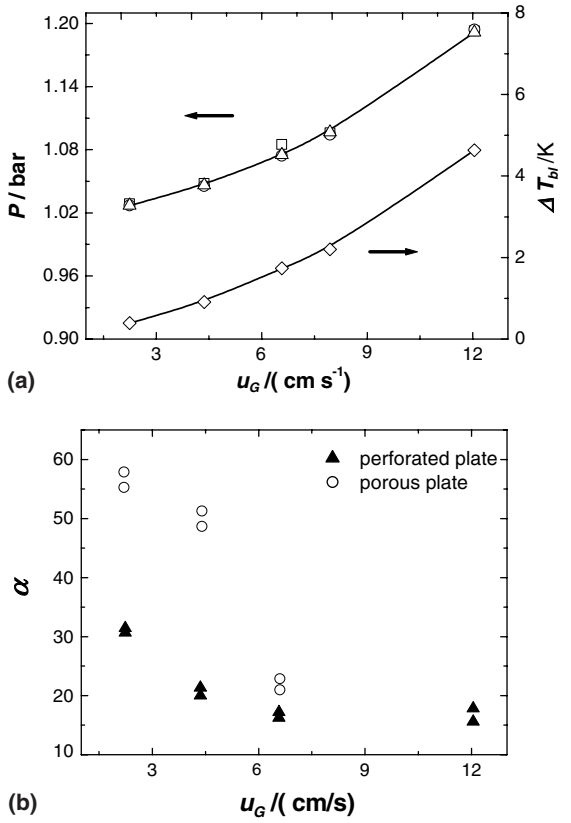

Fig. 3. Effect of the gas superficial velocity upon (a) the evaporator operating pressure and the corresponding boiling point rise and (b) the dimensionless interfacial area for the two analysed spargers. Different symbols refer to duplicates.

determined operating pressure above the normal boiling point was also included in Fig. 3a as a function of u_G. It can be verified that the increase in the quasi-equilibrium value of T_L with increasing u_G in Fig. 2b agrees semi-quantitatively with the boiling point elevation due to the mean operational pressure shown in Fig. 3a.

The changes in the evaporator hydrodynamics as a function of the gas superficial velocity could be qualitatively analysed from the photos of the two-phase mixture. Examples of these photos, as well as the bubble size distributions determined from them are presented elsewhere [18]. For $u_G = 2.2$ cm s^{-1}, there was little variation in the size of the bubbles and these were evenly distributed in the radial position, characterising the homogeneous bubbling regime [14–16]. In contrast, when $u_G = 12.1$ cm s^{-1}, a large variety of bubble sizes was observed, and the existence of a radial gradient in the concentration of bubbles and, accordingly, in the gas hold-up, was evident. These two characteristics point to the heterogeneous bubbling regime.

The bubbling regime can also be characterised by the interfacial area dependency on the sparger, which exists for homogeneous bubbling but not for heterogeneous bubbling. Besides, to the authors' knowledge, although the influence of the sparger on both the hydrodynamics and mass transfer processes for isothermal bubble columns has already been experimentally evaluated [20–23], no such study has been presented so far for direct-contact evaporators. Therefore, apart from the perforated plate, a porous plate was also used as a distributor. In this case, the runs were carried out only for the three lower gas flow rates studied, since no sparger effect was expected for the largest u_G value, which is surely in the heterogeneous bubbling regime. Once again, the experiments were conducted in duplicate and in a random order.

For operation in the quasi-steady-state regime, the d_{32} values reported by Ribeiro and Lage [18] were used to calculate the value of the dimensionless interfacial area for each u_G values and for both spargers. The obtained results are portrayed in Fig. 3b, which clearly shows that the present data includes both the homogeneous and heterogeneous bubbling regime.

Fig. 4 compares the T_L results related to each sparger. For the sake of clarity, the individual runs of a given sparger for the same gas superficial velocity were represented with the same symbol. Regardless of the gas superficial velocity, there seems to be no significant difference between the liquid temperature profiles exhibited using the two different spargers. This agrees with the previous observation that, for a given gas superficial velocity, the liquid temperature at quasi-steady operation was controlled by the evaporator operating pressure which, in turn, was established by the pressure drop in the condensers.

Nevertheless, the significance of the sparger is revealed when one focus his attention on the evaporation rate and bubbling height results, which are respectively shown in Figs. 5 and 6. Once again, for the sake of clearness, results related to duplicates were represented with the same symbol. For the lowest gas superficial velocity, the sparger influence can be noticed. From Figs. 5a and 6a, both the evaporation rate and the bubbling height seem to be higher for the porous plate. Since the liquid mass at the beginning of each run was approximately the same, the bubbling height differences in the initial region of Fig. 6a derive from gas hold-up differences and, therefore, one concludes that the porous plate gives a higher gas hold-up. As evaporation at different rates progresses, the liquid mass in the unit at a given time is no longer the same for the two spargers, so that the bubbling height differences in Fig. 6a start to reflect the combined effects of ε and M_{ev}. On account of the fact that the higher values of ε and M_{ev} are both associated with the same sparger (the porous plate), the H_b curves in Fig. 6a become progressively closer to each other as time goes by.

The analysis of Figs. 5b and 6b reveals that the increase in the gas superficial velocity attenuates the dif-

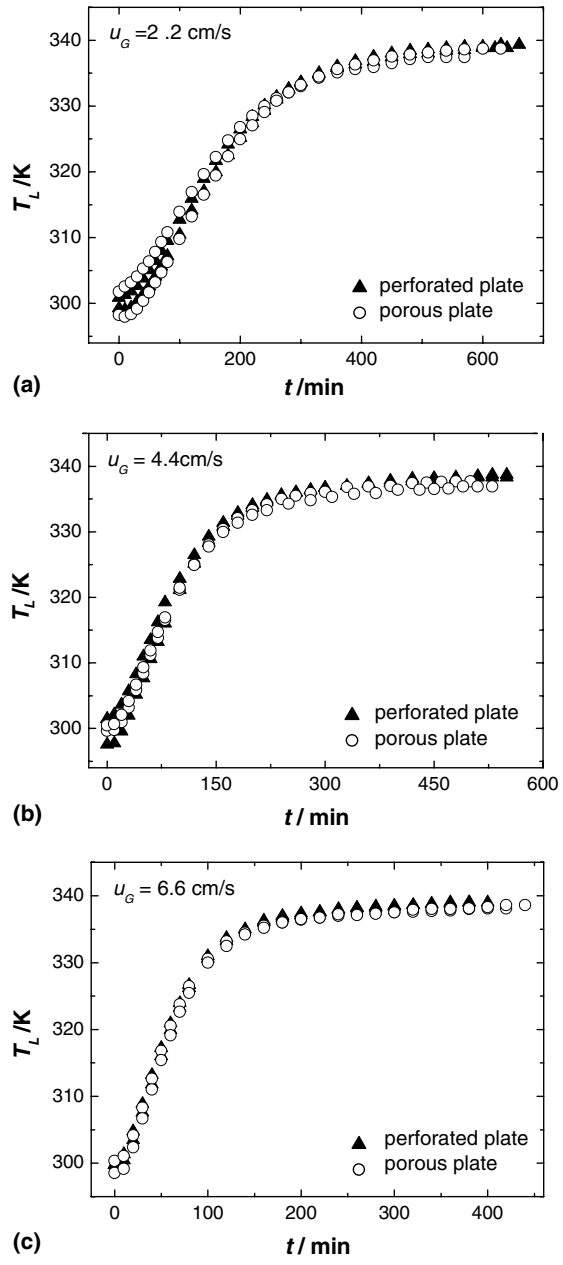

Fig. 4. Comparison between the liquid temperature profiles obtained with two different spargers, considering three gas superficial velocities.

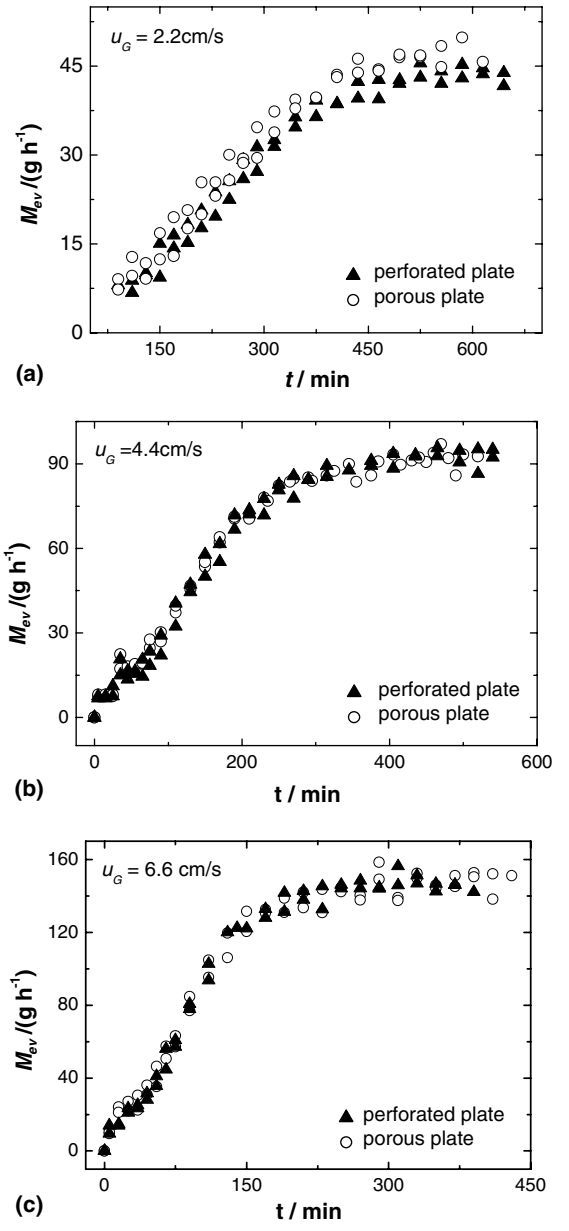

Fig. 5. Evaporation rate as a function of time for the evaporator operating with two different spargers, considering three gas superficial velocities.

ferences between the spargers. Even though the porous plate still seems to give a somewhat higher bubbling height, the evaporation rate results for the two spargers are the same within the data precision. Finally, for $u_G = 6.6$ cm s^{-1}, Figs. 5c and 6c show that the effect of the sparger is completely absent. The differences between the M_{ev} and H_b data for the two spargers are similar to the scatter observed for the two individual runs with the same sparger. Therefore, contrary to what occurred in the previous cases, the gas hold-up, even in the initial instants, did not depend on the sparger type.

Upon considering that the effect of bubble interactions was already important enough to totally suppress the sparger influence for $u_G = 6.6$ cm s^{-1} and that its intensity grows with the gas superficial velocity, one can clearly understand the reason for regarding the

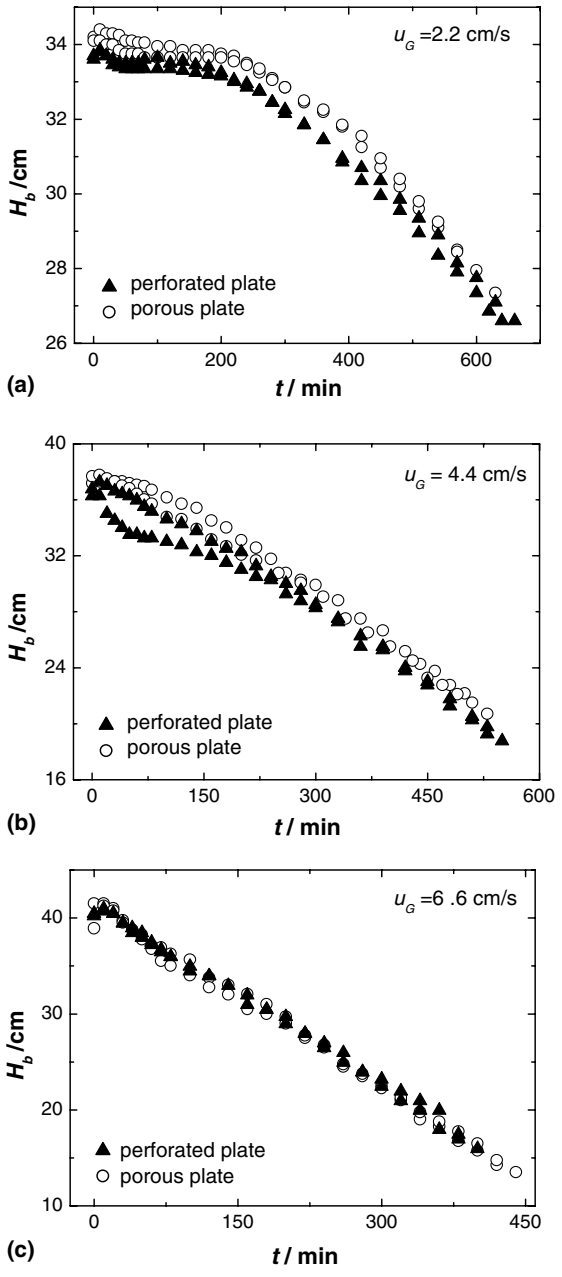

Fig. 6. Bubbling height as a function of time for the evaporator operating with two different spargers, considering three gas superficial velocities.

execution of experimental runs with $u_G > 6.6$ cm s^{-1} for the porous plate as unnecessary.

3.2. Gas hold-up, bubble size distributions and predictions of bubble formation models

Although true that the bubbling height results presented previously already enabled some conclusions to be drawn about the effect of the sparger upon the gas hold-up, new aspects come into evidence when one analyses the gas hold-up values themselves, which are portrayed in Fig. 7 as a function of the operation time for both spargers tested in this work. In this case, for the sake of clarity, only the results from one of the runs for each sparger are presented with error bars. Owing to the intense oscillation of the mixture overall height in the evaporator, which derives from the collapse of the leaving bubbles, the gas hold-up values determined by the bed expansion method bear a considerable experimental deviation (about 20%). It ought to be emphasised, though, that the differences between the values related to the duplicates were usually lower than 5%, the only exception being the runs for the perforated plate with $u_G = 4.4$ cm s^{-1}, whose discrepancy in the transient region of the curves is somewhat high, a fact which may be related to unnoticed oscillations in the air line which fed the evaporator, since the data for the two runs agree quite well in the quasi-steady-state region. Regardless of the sparger and despite the experimental deviation, the data do exhibit the well-known trend of gas hold-up increase with u_G which is characteristic of bubble columns [24].

The effect of the sparger upon the gas hold-up is now clearly seen in Fig. 7. Confirming the previous conclusions, for $u_G = 2.2$ cm s^{-1}, when the equipment operates in the homogeneous regime, at which coalescence frequencies are low, the sparger whose orifice diameter is smaller, that is, the porous plate, leads to higher gas hold-up values due to the formation of smaller bubbles. As the gas flow rate increases, the coalescence frequencies grow accordingly, and the bubble formation diameter becomes progressively less important, so that the gas hold-up curves for the two spargers become closer and end up equal for $u_G = 6.6$ cm s^{-1}, which points to the heterogeneous bubbling regime.

The new aspect to which attention should be drawn in Fig. 7 is the particular shape of the gas hold-up profiles. For the perforated plate, regardless of the gas superficial velocity, there is always an increase in ε at the very beginning of the operation, followed by a decrease, after which an equilibrium value is reached in the quasi-steady-state regime. On the other hand, for the porous plate, such a profile is only exhibited when $u_G = 6.6$ cm s^{-1}. In the case of the other two tested gas superficial velocities, after the decrease region, the gas hold-up seems to increase again before reaching its equilibrium value in the quasi-steady-state regime.

Immediately after the beginning of the gas injection, the first-formed bubbles ascend through an almost quiescent liquid, their drag being responsible for the liquid acceleration to establish a circulation inside the column. Since the subsequent bubbles have to move against the returning liquid, their ascension velocity is reduced. Therefore, the establishment of the liquid circulation

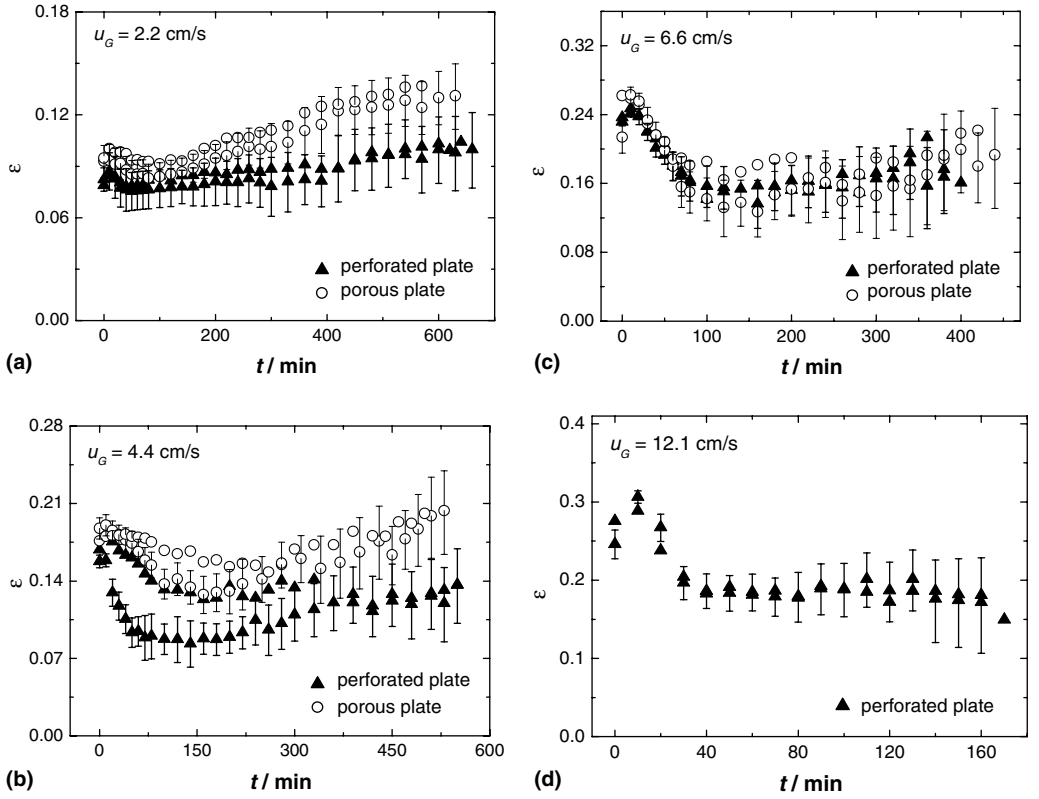

Fig. 7. Evolution of the gas hold-up in the evaporator as a function of the operating time for different gas superficial velocities, considering two different spargers.

pattern should be responsible for the initial gas-hold increase observed in Fig. 7a–d.

As regards the region of gas hold-up decrease, it can be seen in Fig. 7 that, although less important for $u_G = 2.2$ cm s^{-1}, this region is quite evident for the other gas superficial velocities. In these cases, the extent of this region diminishes as u_G is raised. These evidences suggest that this gas hold-up decrease would be related to the evolution of coalescence phenomena and the resulting temporal change of the bubble size distribution. With the aim of verifying this possibility, the photos of the two-phase mixture taken during the runs were analysed to determine the bubble size distributions. In Fig. 8, the results (in terms of the relative frequency, RF) obtained for an operating time of 10 min are compared with the ones reported by Ribeiro and Lage [18] for the operation in the quasi-steady-state regime. Corroborating the formulated hypothesis, whichever the sparger, a pronounced discrepancy between the bubble size distributions for the initial and final instants is observed for the two higher u_G values (Fig. 8a–c). For $t = 10$ min, the distribution is unimodal, with a reduced size range and a high fraction of smaller bubbles, whereas, in the quasi-steady-state regime, the distribution becomes bimodal, and widens considerably, including sizes which were previously unobserved. Upon comparing the experimental profiles of gas hold-up and liquid temperature, one notices that the periods of time in which the gas hold-up decreased are the same for which fast liquid temperature changes were observed. Consequently, these observed changes in the coalescence frequency may be related to liquid temperature variations, being, thus, an exclusive feature of transient non-isothermal bubbling. It should be emphasised that experimental evidences in support of the augmentation of the bubble coalescence rate with an increase in the liquid temperature have already been reported in the literature [25,26].

Considering now the region of gas hold-up increase exhibited by the porous plate for the two lower gas flow rates (Fig. 7a and b), a similar reasoning reveals that such behaviour should necessarily be associated with a diminution of bubble sizes. For the lowest gas superficial velocity, the bubble size distributions related to an operating time equal to 10 min, determined in this work, are compared in Figs. 8d and e with the ones reported by Ribeiro and Lage [18] for operation in the quasi-steady-state regime. In perfect agreement with the gas hold-up

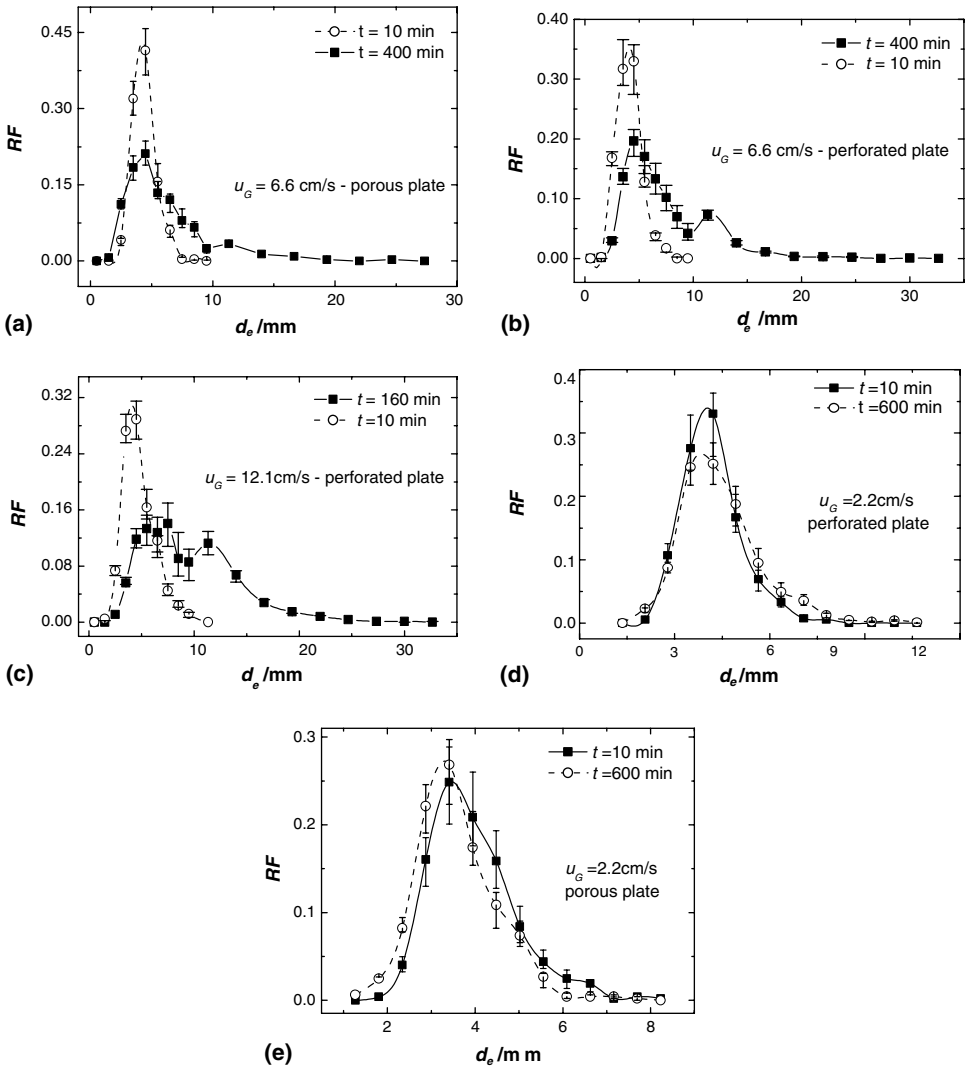

Fig. 8. Comparison between the bubble size distributions determined in this work for an operating time of 10 min and the ones reported by Ribeiro and Lage [18] for the quasi-steady-state regime.

results, with the porous plate as sparger, the final bubble size distribution is clearly shifted to the left, towards smaller diameters, in relation to the initial one, whereas, for the perforated plate, no significant difference between the size distributions can be perceived within the data precision, as an intersection between the ranges of relative frequency is verified for most bubble classes.

This similarity of bubble size distributions for the perforated plate when $u_G = 2.2$ cm s^{-1} evidences that coalescence phenomena, which should have been enhanced by the increase in the liquid temperature as previously observed for higher gas flow rates, do not play an important role. Thus, the mean bubble diameter at any given height above the sparger should be similar to the mean bubble diameter generated at the sparger and, therefore, could be satisfactorily predicted by a suitable bubble formation model. In Table 1, the volumetric mean bubble diameters (d_{30}) determined for the perforated plate based upon the size distributions are compared with the ones predicted by the application of Campos and Lage's [27] formulation to the Davidson and Schüler's [28] isothermal bubble formation model (DS) in order to account for heat and mass transfer effects during the formation of superheated bubbles. The agreement between calculated and experimental values is rather consistent with the mean prediction error reported by Jamialahmadi et al. [29] for the Davidson and Schüler's model [28], namely 18%. However, the predicted diameters are all lower than the experimental values, which could either be an indication of coales-

Table 1
Comparison between experimental mean bubble diameters (d_{30}) and bubble diameters predicted by correlations (d_{cor}) and by non-isothermal (Campos and Lage [27]) and isothermal (Bowonder and Kumar [38]) bubble formation models (d_{bf})

Perforated plate ($u_G = 2.2$ cm s^{-1})						
t/min	d_{30}/mm	d_{bf}/mm (Campos and Lage [27])		$(d_{30} - d_{bf})/d_{30} \times 100$		
		DS[a]	MDS[b]	DS[a] [28]	MDS[b]	
10	4.4 ± 0.1	3.6	4.3	18	2.3	
600	4.9 ± 0.1	4.1	4.6	19	6.1	
	4.7 ± 0.1			15	2.1	
Porous plate ($u_G = 2.2$ cm s^{-1})						
		d_{bf}/mm (Bowonder and Kumar [38])			d_{cor}/mm	
		RA[c] [39]	G&V[d] [40]	JA[e] [29]	K1 [f][34]	K2 [f] [35]
10	4.2 ± 0.1	1.16	0.75	1.06	2.28	4.23
600	3.8 ± 0.1	1.16	0.72	1.02	2.22	4.31

[a] Davidson and Schüler [28] bubble formation model.
[b] Modified Davidson and Schüler bubble formation model with surface tension effect.
[c] Ramakrishnan et al. [39] bubble formation model.
[d] Gaddis and Vogelpohl [40] bubble formation model.
[e] Jamialahmadi et al. [29] bubble formation model.
[f] Koide et al. [34,35] correlations for the size of bubbles formed at porous plates.

cence effects during bubbles ascension or a consequence of neglecting the surface tension effect in the original Davidson and Schüler's bubble formation model [28]. This effect is actually known to be quite important in bubble formation for low gas flow rates [30,31]. In order to settle this matter, the Campos and Lage [27] formulation was also applied to a modified Davidson and Schüler model (MDS), into which the surface tension force was included, considering a contact angle equal to 52°, a mean of the experimental results reported by Kandlikar and Steinke [32] for stainless steel with different surface roughness. The obtained results are also presented in Table 1. When the surface tension effect during bubble formation is taken into account, a much better agreement between experimental and predicted mean bubble diameters is observed, corroborating, therefore, the hypothesis of negligible coalescence during bubble ascension for $u_G = 2.2$ cm s^{-1}.

For the porous plate, the experimental values of d_{30} are also listed in Table 1. Upon comparing these results with those for the perforated plate, one notices that initially, at $t = 10$ min, there is little difference between the two spargers, but, for operation in the quasi-steady-state regime, the porous plate gives a considerably smaller mean bubble size, both facts being in conformity with the gas hold-up results in Fig. 7a. Since it was concluded that coalescence during bubble ascension was not important for $u_G = 2.2$ cm s^{-1}, the differences among the spargers must derive from the formation stage. However, for the same bubbling conditions, smaller orifices inevitably generate smaller bubbles, so that the similarity between the spargers observed for $t = 10$ min can only be explained by coalescence of adjacent bubbles during the formation stage on or near the porous plate, a phenomenon which has already been reported in the literature [33,34].

The most common quantitative approach which has been adopted so far when it comes to porous spargers seems to be the establishment of empirical correlations for the mean bubble size. Apparently, from the available equations [34–37], only the ones proposed by Koide et al. [34,35] included in their range of applicability the conditions related to this work. The earlier correlation [34] (K1) was developed based upon data for seven different liquids and has a mean error of 25.4%. The other correlation [35] (K2) is only valid for water and its mean error equals 8.2%. Their predictions are also included in Table 1. With regard to bubble formation models for porous plates, the formulation of Bowonder and Kumar [38], based on a general model for bubble formation at an isolated orifice and on the assumption of a close hexagonal packed arrangement of the formed bubbles, is, to the authors' knowledge, the only option available in the literature. In this work, three different relations were used in Bowonder and Kumar [38] formulation for calculating the diameter of the bubbles generated by the porous plate: the one proposed by Ramakrishnan et al. [39] (RA), originally adopted by Bowonder and Kumar [38], the one elaborated by Gaddis and Vogelpohl [40] (G&V), which has been recommended by Pinto [31] for low gas flow rates, and the one presented by Jamialahmadi et al. [29] (JA), whose mean deviation is claimed to be smaller than the one associated with the Gaddis and Vogelpohl model

[40]. The corresponding results are all presented in Table 1. Neither the mean bubble diameter correlations nor the bubble formation models used for the porous plate take into account heat and mass transfer effects. In all calculations, in view of the high thermal efficiency of direct-contact evaporators, the gas temperature was assumed to be equal to the liquid one, a procedure which has already been shown to provide reasonably good results for the estimation of mean bubble size in non-isothermal bubbling using isothermal bubble formation models for perforated plates [41].

As shown in Table 1, the mean bubble diameters predicted with the correlation of Koide et al. [34] are always smaller than the experimental values. A similar trend was originally reported by Koide et al. [34] when their correlation was tested against the experimental data of Houghton et al. [42] for isothermal bubbling and might be related to differences in the experimental apparatus. Both in this work and in the one reported by Houghton et al. [42], the bubbling column and the gas distributor had the same diameter, whereas the dimensions of the bubbling cell employed by Koide et al. [34] were far greater than the sparger diameter. In the latter case, the probability of bubble coalescence over the distributor is reduced in comparison with the former, due to the available region for dispersing the formed bubble swarm during its ascension, which, in turn, accounts for the smaller bubble diameters. On the other hand, a good agreement is verified between the experimental data and the predictions of the correlation of Koide et al. [35], specially at $t = 10$ min, when the liquid temperature (300 K) is close to the value associated with the data used in the correlation development (293 K) and heat and mass transfer effects are reduced due to the small temperature difference between the liquid and the inlet gas (the T_G^{in} behaviour for the porous plate sparger is quite similar to that represented in Fig. 2c for the perforated plate distributor). This is a strong evidence in favour of the hypothesis of coalescence on or near the porous plate during bubble formation, since the experimental values were shown to be not only consistent with independent gas hold-up measurements but also in agreement with the predictions of a literature correlation.

The bubble formation diameters predicted by the model of Bowonder and Kumar [38], however, regardless of the relation employed for calculating the diameter of the bubbles generated at a single orifice, are always much smaller than the experimental mean bubble diameters. Even though their predictions are poor, most bubble size results from the formation models do exhibit the reduction trend for bubble diameter as the liquid temperature is increased, corroborating, thus, the tendency verified with the measured bubble size distributions. Such trend is also perceived in the results from the correlation of Koide et al. [34] which was established using data for different liquids and, hence, include somehow physical property effects. Taking into account the fact that only data for water at 293 K were employed in the development of the Koide et al. [35] correlation, it is natural to expect its failure in accounting for physical property effects upon the bubble diameter, and, consequently, it does not predict the experimentally observed tendency.

3.3. Interfacial area and thermal analysis

For very small bubbling heights in a direct-contact evaporator, there is not enough contact time and/or interfacial area to establish equilibrium between the outlet gas stream and the liquid phase. In this case, the interfacial area influences the heat and mass processes in the unit, leading, thereby, to changes in its thermal efficiency. In this final section, an analysis of these aspects for the considered experimental unit is presented.

Considering the bubble diameter and gas hold-up data, the interfacial area behaviour shown in Fig. 3b can now be clearly understood. Whichever the gas flow rate, the bubbles formed at the porous plate will always be smaller than the ones formed at the perforated plate, since the orifice mean diameter of the former (12 μm) is considerably smaller than that of the latter (0.5 mm). For the homogeneous regime, this difference tends to be maintained along the ascension stage because coalescence frequencies are small. A smaller mean bubble diameter implies smaller bubble terminal velocity and, thus, a higher gas hold-up. For the two lower values of u_G, the synergistic combination of lower mean diameter and higher gas hold-up associated with the porous plate sparger leads to a significant increase in the superficial area in relation to the perforated plate sparger. This effect is especially high for $u_G = 4.4$ cm s^{-1}, when the value of α associated with the porous plate is more than twice as high as the one related to the perforated plate. Considering that this value of u_G is close to the one associated with the bubbling regime transition and that porous spargers are known to stabilise operation in the homogeneous regime to a greater extent than perforate ones [21,24], the prominent difference of α values between the two spargers observed for $u_G = 4.4$ cm s^{-1} might be related to a difference in the bubbling regime. With the perforated plate, operation might have taken place at the beginning of the homogeneous–heterogeneous transition region, and bubble coalescence phenomena, therefore, started to acquire importance, whereas, with the porous plate, the homogeneous regime might still have been observed, reducing to a minimum, thus, the influence of bubble coalescence phenomena. This hypothesis is reinforced by the fact that the value of α for the perforated plate decreased 33% when u_G varied from 2.2 to 4.4 cm s^{-1}, while, for the porous plate, the same variation of u_G led to a reduction of only 11% in the α value. On the other hand, the two spargers give

fairly similar values of interfacial area when $u_G = 6.6$ cm s^{-1}, evidencing the dominant effect of bubble coalescence and breakage phenomena associated with the heterogeneous bubbling regime. Furthermore, an almost twofold further increase in the value of u_G did not seem to produce any substantial variation in α, indicating that the interfacial area tends towards a stabilisation value controlled by the bubble interaction phenomena. Thus, for $u_G = 6.6$ and 12.2 the evaporator operates in the heterogeneous bubbling regime. It should be emphasised that these considerations are all confirmed by the bubble size distribution data reported by Ribeiro and Lage [18] for the operating conditions analysed in this work.

The thermal efficiency changes with u_G for a given sparger can be assessed in terms of the gas outlet temperature, T_G^{out}. Fig. 9 shows the evolution of the difference between the liquid temperature and the gas outlet temperature as a function of time for the unit operating with the perforated plate for the several values of u_G. Once again, filled and open symbols with the same geometrical shape refer to duplicates. Whichever the value of u_G, the gas outlet temperature, measured at the top of the column, was almost always lower than the liquid-phase temperature. Therefore, it is concluded that, at the time of disengagement, both liquid and gas phases were basically at the same temperature, being the heat losses in the freeboard region of the equipment responsible for the further drop in the value of T_G^{out}. Since conduction in the insulating glass fibre piece around the column was the main resistance for heat transfer, these heat losses were not a strong function of u_G, so that the higher the value of u_G, the lower the reduction in the gas outlet temperature, as evidenced in Fig. 9. A similar behaviour was observed for operation with the porous plate.

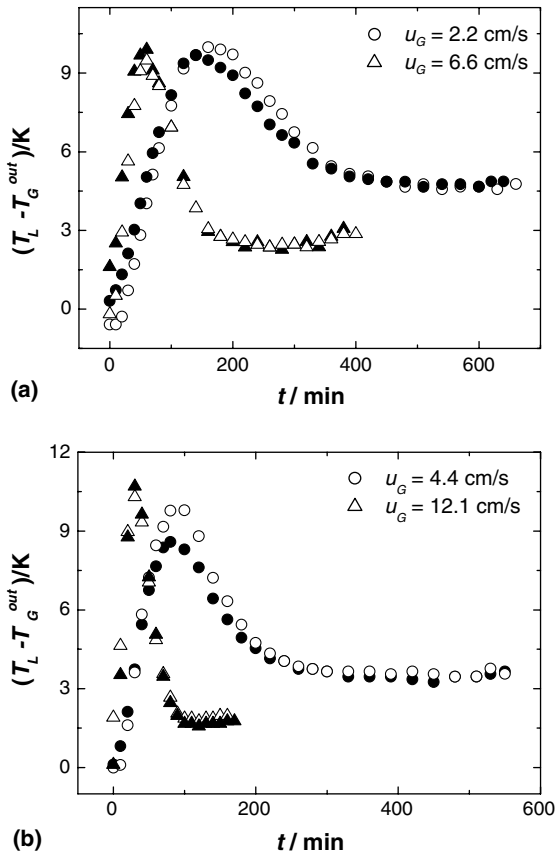

Fig. 9. Variation of the temperature difference between the liquid and the outlet gas as a function of time for operation with the perforated plate and different gas superficial velocities (open and filled symbols refer to duplicates).

The results in Fig. 9 reveal that, despite the abrupt drop in the evaporator available area which accompanies the bubbling regime transition, no change was observed in the unit thermal efficiency, as all energy contained in the injected gas was transferred to the liquid. Therefore, the evaporation rate was actually limited by the amount of available energy and not by the interfacial area. In other words, for all u_G values tested, should the gas inlet temperature be higher, an even larger evaporation rate could have been obtained.

The above analysis also implies that the vaporisation rate should be independent of the sparger. However, Fig. 5a shows that, at the pseudo steady-state regime, M_{ev} for the porous plate is about 7% larger than the value for the perforated plate. As all the available heat was drawn from the gas stream, this differences in M_{ev} should derive from differences in the heat transferred through the gas distribution system.

Following the procedure previously described in Section 2.2, the Q_d and Q_G values and their 95% confidence intervals were determined for each individual run at the quasi-steady-state regime. As U_p does not depend upon u_G, its value was experimentally determined for a single value of u_G, namely 6.6 cm s^{-1}, giving (1.6 ± 0.2) W m^{-2} K^{-1}, and afterwards used in the calculation of Q_p for all other runs. Once Q_d, Q_G and Q_p were known, they were added up to give the total amount of heat transfer to the liquid (Q_T). The obtained results are listed in Table 2. Also shown in this table is the fraction of Q_T lost to the surroundings through the walls. These data demonstrate that, although the contribution of Q_G clearly increases with u_G, up to 64% of the total amount of energy received by the liquid may be transferred through the sparger in the experimental configuration analysed.

The difference in the vaporisation rates between the runs with the different spargers for the lowest u_G value can now be analysed. The increase in the vaporisation rate for the porous sparger by 7% (Fig. 5a) is a result of a corresponding 7% augmentation of Q_T, which comes entirely from a 13% increase of Q_d (Table 2). Defining the overall heat-transfer coefficient through the gas distributor, U_d, using the difference between a mean gas

Table 2
Heat-transfer rates at the quasi-steady-state regime

u_G/(cm s^{-1})	Q_T/W	Contributions to Q_T		(Q_p/Q_T)/%
		Q_G/W (Q_G/Q_T/%)	Q_d/W (Q_d/Q_T/%)	
Perforated plate				
2.2	39.8 ± 1.0	16.8 ± 0.1 (42)	23.1 ± 0.9 (58)	11
	42.5 ± 0.9	17.1 ± 0.1 (40)	24.4 ± 0.8 (60)	10
4.4	76 ± 1	29.8 ± 0.2 (39)	46 ± 1 (61)	4
	74 ± 2	29.6 ± 0.1 (40)	45 ± 2 (60)	5
6.6	112 ± 4	55.1 ± 0.2 (49)	56 ± 3 (51)	3
	109 ± 1	54.6 ± 0.1 (50)	55 ± 1 (50)	3
12.1	211 ± 4	136.8 ± 0.7 (65)	74 ± 3 (35)	2
	217 ± 10	139.4 ± 0.6 (64)	78 ± 9 (36)	2
Porous plate				
2.2	43.2 ± 0.9	16.7 ± 0.1 (39)	26.5 ± 0.9 (61)	10
	44.6 ± 1.4	16.1 ± 0.2 (36)	28.5 ± 1.3 (64)	10
4.4	73.2 ± 3.7	26.3 ± 0.1 (36)	46.9 ± 3.5 (64)	5
	73.2 ± 0.4	29.8 ± 0.1 (41)	43.4 ± 0.4 (59)	5
6.6	111 ± 2	49.7 ± 0.2 (45)	62 ± 2 (55)	3
	108 ± 3	54.4 ± 0.1 (50)	54 ± 3 (50)	3

temperature before the sparger and the liquid temperature, it could be shown that this larger Q_d for the porous plate sparger at $u_G = 2.2$ cm s^{-1} came from a 16% increase in U_d. Since the U_d values for both spargers agree within their determination error for the other values of u_G, this increase in U_d for the porous plate has to be related to a larger convection coefficient on the liquid side.

4. Conclusions

The dynamic operation of a direct-contact evaporator was experimentally characterised with the air–water system for both homogeneous and heterogeneous bubbling regimes. The evaporation rate was shown to increase with the gas superficial velocity while the quasi-steady liquid temperature was shown to be controlled by the evaporator operating pressure. For operation at the homogeneous bubbling regime, a sparger with a lower orifice diameter led to smaller mean bubble diameters and higher values of gas hold-up. The synergistic combination of these two factors brought about a remarkable augmentation of the interfacial area in the evaporator. However, as the gas superficial velocity was raised, this sparger effect was gradually reduced and eventually disappeared for operation at the heterogeneous bubbling regime, when the same interfacial area was observed regardless of the sparger due to the coalescence effects.

Provided that the gas superficial velocity was high enough to prevent operation at the homogeneous regime, whichever the sparger, the dynamic gas hold-up profiles always exhibited a declining region before the quasi-steady-state equilibrium value was reached. This region was shown to be related to a temporal evolution of the bubble size distributions due to the increase in the coalescence frequencies which was caused by the augmentation of the liquid temperature. For the perforated plate operating in the homogeneous bubbling regime, bubble coalescence during the ascension stage was proven to be negligible, as no differences between the initial and final bubble size distributions could be detected and the mean bubble diameters were well predicted by the application of Campos and Lage's [27] heat and mass transfer formulation to a modified Davidson and Schüler's model [28] which takes surface tension effects into account.

With regard to the porous plate, the bubble size distribution measured at the first 10 min of operation bore a strong resemblance to the one obtained for the perforated plate. Moreover, the corresponding experimental mean bubble diameter was found to be much greater than the one predicted with the bubble formation model of Bowonder and Kumar [38] for porous plates. These facts were considered to be evidences of coalescence on or near the porous plate surface during the bubble formation stage. Compared to its initial value, the size distribution at the quasi-steady-state was shifted towards smaller bubbles and, accordingly, a region where the gas hold-up increases exists previously to the establishment of its quasi-steady value. This bubble size reduction trend was observed to be in agreement with the predictions of the empirical mean bubble size

correlation of Koide et al. [34] and also with the predictions of most of tested the bubble formation models. Although giving predictions in better agreement with the experimental mean bubble diameters, Koide et al. [35] correlation does not show the observed bubble size reduction trend.

The homogeneous–heterogeneous bubbling regime transition was shown to be accompanied by an abrupt drop in the available area for heat and mass transfer in the evaporator. Nonetheless, despite this drop, all energy transported by the gas as sensible heat could be transferred to the liquid, so that the evaporation rate was actually controlled by the available energy amount and not by the interfacial area, a result which clearly illustrated the high thermal efficiency of direct-contact units. For the studied unit, depending upon the gas superficial velocity, from 35% to 64% of the total amount of energy received by the continuous phase was transferred through the gas distribution system. An increase in the convection coefficient on the liquid side of the sparger was found to be the cause of a small increase in the vaporisation rate for the lowest superficial velocity when the porous sparger was used.

Acknowledgements

The authors would like to thank CNPq (grant no. 550614/02-8) and FAPERJ (E-26/170.420/99-APQ1) for the financial support provided.

References

[1] R.F. Boehm, F. Kreith, Direct-Contact Heat Transfer, Hemisphere, New York, 1988, 1–24.
[2] H.R. Jacobs, Direct-contact heat transfer for process technologies, Journal of Heat Transfer 110 (4b) (1988) 1259–1270.
[3] C.S. Cronan, Submerged combustion flares a new, Chemical Engineering 63 (2) (1956) 163–167.
[4] A. Williams, Submerged combustion for water plants, Mechanical Engineering 87 (7) (1965) 34–37.
[5] E.M. Burdick, C.O. Anderson, W.E. Duncan, Application of submerged combustion to processing of citrus waste products, Chemical Engineering Progress 45 (9) (1949) 539–544.
[6] A.H. Luedicke Jr., B. Hendrickson, G.M. Pigott, A method for the concentration of proteinaceous solutions by submerged combustion, Journal of Food Science 44 (1979) 1469–1473.
[7] K.A. Kobe, F.H. Conrad, E.W. Jackson, Evaporation by submerged combustion—I. Experimental equipment, Industrial and Engineering Chemistry 25 (9) (1933) 984–987.
[8] K.A. Kobe, F.H. Conrad, E.W. Jackson, Evaporation by submerged combustion—II. Sulfite waste liquor, Industrial and Engineering Chemistry 25 (9) (1933) 987–989.
[9] J.J. Owen Jr., W.A. Moggio, Submerged combustion evaporation of neutral sulphite spent cooking liquor, TAPPI Journal 38 (2) (1955) 144–147.
[10] P.M. Rao, P.D. Sunavala, Concentration of black liquor by submerged combustion technique, Indian Journal of Technology 20 (1982) 56–59.
[11] P.A. Iyer, C. Chu, Submerged combustion, Desalination 9 (1) (1971) 19–31.
[12] J. Kawasaki, T. Hayakawa, Direct-contact mass and heat transfer between vapour and liquid with change of phase, Journal of Chemical Engineering of Japan 5 (2) (1972) 119–124.
[13] E.M. Queiroz, Simultaneous heat and mass transfer in bubbling processes, D.Sc thesis, PEQ/COPPE/UFRJ, Rio de Janeiro, RJ, 1990 (in Portuguese).
[14] T. Maruyama, S. Yoshida, T. Mizushina, The flow regime transition in a bubble column, Journal of Chemical Engineering of Japan 14 (1981) 352–357.
[15] H.T. Bi, J.R. Grace, Regime transitions: analogy between gas-liquid cocurrent upward flow and gas-solid upward transport, International Journal of Multiphase Flow 22 (2000) 1–19.
[16] M.C. Ruzicka, J. Zahradnik, J. Drahos, N.H. Thomas, Homogeneous–heterogeneous regime transition in bubble columns, Chemical Engineering Science 56 (2001) 4609–4626.
[17] T.J. Nelson, Tnimage Scientific Image Analysis Software Transforming and Numeric Image Analysis System (Linux version), 2000, ftp://sunsite.unc.edu/pub/linux/apps/graphics/misc/.
[18] C.P. Ribeiro Jr., P.L.C. Lage, Experimental study on bubble size distributions in a direct-contact evaporator, Brazilian Journal of Chemical Engineering 21 (1) (2004) 69–81.
[19] R.B. Bird, W.E. Stewart, E.N. Lightfoot, Transport Phenomena, John Wiley, Singapore, 1960, p. 182.
[20] C. Guy, P.J. Carreau, J. Paris, Mixing characteristics and gas hold-up of a bubble column, The Canadian Journal of Chemical Engineering 64 (1986) 23–35.
[21] G. Hebrard, D. Bastoul, M. Roustan, Influence of the gas sparger on the hydrodynamic behaviour of bubble columns, Chemical Engineering Research and Design 74 (1996) 406–414.
[22] E. Camarasa, C. Vial, S. Poncin, G. Wild, N. Midoux, J. Bouillard, Influence of coalescence behaviour of the liquid and of gas sparging on hydrodynamics and bubble characteristics in a bubble column, Chemical Engineering and Processing 38 (1999) 329–344.
[23] M. Bouaifi, G. Hebrard, D. Bastoul, M. Roustan, A comparative study of gas hold-up, bubble size, interfacial area and mass transfer coefficients in stirred gas–liquid reactors and bubble columns, Chemical Engineering and Processing 40 (2001) 97–111.
[24] Y.T. Shah, B.G. Kelkar, S.P. Godbole, W.-D. Deckwer, Design parameters estimations for bubble column reactors, AIChE Journal 28 (1982) 353–379.
[25] R.R. Lessard, S.A. Zieminski, Bubble coalescence and gas transfer in aqueous electrolytic solutions, Industrial and Engineering Chemistry Fundamentals 10 (2) (1971) 260–269.
[26] G.S. Grover, C.V. Rode, R.V. Chaudhari, Effect of temperature on flow regimes and gas hold-up in a bubble

column, The Canadian Journal of Chemical Engineering 64 (3) (1986) 501–504.
[27] F.B. Campos, P.L.C. Lage, Heat and mass transfer modelling during the formation and ascension of superheated bubbles, International Journal of Heat and Mass Transfer 43 (16) (2000) 2883–2894.
[28] J.F. Davidson, B.O.G. Schüler, Bubble formation at an orifice in a viscous liquid, Transactions of the Institution of Chemical Engineers 38 (1960) 144–154.
[29] M. Jamialahmadi, M.R. Zehtaban, H. Müller-Steinhagen, A. Sarrafi, J.M. Smith, Study of bubble formation under constant flow conditions, Chemical Engineering Research & Design 79 (A5) (2001) 523–532.
[30] R. Kumar, N.R. Kuloor, The formation of bubbles and drops, Advances in Chemical Engineering 8 (1970) 255–368.
[31] A.D. Pinto, Bubble formation at orifices: initial evaporation in bubbling processes, M.Sc Dissertation, PEQ/COPPE/UFRJ, Rio de Janeiro, RJ, 1990 (in Portuguese).
[32] S.G. Kandlikar, M.E. Steinke, Contact angles and interface behaviour during rapid evaporation of liquid on a heated surface, International Journal of Heat and Mass Transfer 45 (18) (2002) 3771–3780.
[33] H. Vershoor, Some aspects of the motion of a swarm of gas bubbles rising through a vertical liquid column, Transactions of the Institution of Chemical Engineers 28 (1950) 52–57.
[34] K. Koide, S. Kato, Y. Tanaka, H. Kubota, Bubbles generated from porous plates, Journal of Chemical Engineering of Japan 1 (1) (1968) 51–56.
[35] K. Koide, T. Hayashi, M. Noro, Y. Takemura, N. Kawamata, H. Kubota, Bubbles generated from porous plates in pure liquid and in aqueous solutions of inorganic electrolytes, Journal of Chemical Engineering of Japan 5 (3) (1972) 236–242.
[36] T. Hayashi, K. Koide, T. Sato, Bubbles generated from porous plates in organic solutions and aqueous solutions of organic substances, Journal of Chemical Engineering of Japan 8 (1) (1975) 16–20.
[37] T. Miyahara, A. Tanaka, Size of bubbles generated from porous plates, Journal of Chemical Engineering of Japan 30 (2) (1997) 335–353.
[38] B. Bowonder, R. Kumar, Studies in bubble formation—IV Bubble formation at porous discs, Chemical Engineering Science 25 (1970) 25–32.
[39] S. Ramakrishnan, R. Kumar, N.R. Kuloor, Studies in bubble formation—I Bubble formation under constant flow conditions, Chemical Engineering Science 24 (4) (1969) 731–747.
[40] E.S. Gaddis, A. Vogelpohl, Bubble formation in quiescent liquids under constante flow conditions, Chemical Engineering Science 41 (1) (1986) 97–105.
[41] L.F.L.R. Silva, P.L.C. Lage, Gas hold-up and bubble sizes in non-isothermal bubble columns, in: J.T. Freire (Ed.), Proceedings of the Twenty-eighth Brazilian Congress on Particulate Systems, COPPE/UFRJ, Teresópolis, 2000, pp. 207–214 (in Portuguese).
[42] G. Houghton, A.M. McLean, P.D. Ritchie, Mechanism of formation of gas bubble-beds, Chemical Engineering Science 7 (1–2) (1957) 40–50.